An efficient computational approach for control of nonlinear transient responses of smart piezoelectric composite plates

ARTICLE *in* INTERNATIONAL JOURNAL OF NON-LINEAR MECHANICS · JUNE 2015

Impact Factor: 1.46 · DOI: 10.1016/j.ijnonlinmec.2015.06.003

8 AUTHORS, INCLUDING:

Tien Dung Dinh
Ghent University
3 PUBLICATIONS **1** CITATION
SEE PROFILE

Chien thai Hoang
Ton Duc Thang University
30 PUBLICATIONS **383** CITATIONS
SEE PROFILE

Hung Nguyen-Xuan
Ho Chi Minh City University of Science
127 PUBLICATIONS **2,438** CITATIONS
SEE PROFILE

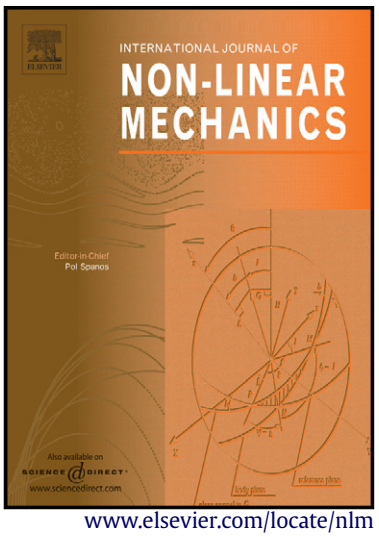

www.elsevier.com/locate/nlm

An efficient Computational approach for control of nonlinear transient responses of smart piezoelectric composite plates

P. Phung-Van, Lieu B. Nguyen, Loc V. Tran, T.D. Dinh, Chien H. Thai, S.P.A. Bordas, M. Abdel-Wahab, H. Nguyen-Xuan

PII: S0020-7462(15)00113-4
DOI: http://dx.doi.org/10.1016/j.ijnonlinmec.2015.06.003
Reference: NLM2500

To appear in: *International Journal of Non-Linear Mechanics*

Received date: 6 March 2015
Revised date: 2 May 2015
Accepted date: 4 June 2015

Cite this article as: P. Phung-Van, Lieu B. Nguyen, Loc V. Tran, T.D. Dinh, Chien H. Thai, S.P.A. Bordas, M. Abdel-Wahab, H. Nguyen-Xuan, An efficient Computational approach for control of nonlinear transient responses of smart piezoelectric composite plates, *International Journal of Non-Linear Mechanics,* http://dx.doi.org/10.1016/j.ijnonlinmec.2015.06.003

An efficient computational approach for control of nonlinear transient responses of smart piezoelectric composite plates

P. Phung-Van[1], Lieu B. Nguyen[2], Loc V. Tran[1], T. D. Dinh[3],
Chien H. Thai[4], S.P.A. Bordas[5], M. Abdel-Wahab[1,*], H. Nguyen-Xuan[6,7,*]

[1]*Department of Mechanical Construction and Production, Faculty of Engineering and Architecture, Ghent University, Belgium*
Email: P. Phuc-Van (phuc.phungvan@ugent.be), M. Abdel-Wahab (magd.abdelaahab@ugent.be)

[2]*Faculty of Civil and Applied Mechanics, University of Technical Education Ho Chi Minh City, Vietnam*
[3]*Department of Materials Science and Engineering, Faculty of Engineering and Architecture, Ghent University, Belgium*
[4]*Division of Computational Mechanics, Ton Duc Thang University, Vietnam*
[5]*Université du Luxembourg, Faculté des Sciences, Luxembourg*
[6]*Department of Architectural Engineering, Sejong University, Seoul, South Korea*
[7]*Department of Computational Engineering, Vietnamese-German University, Vietnam*

ABSTRACT

An efficient computational approach based on a generalized unconstrained approach in conjunction with isogeometric analysis (IGA) are proposed for dynamic control of smart piezoelectric composite plates. In composite plates, the mechanical displacement field is approximated according to the proposal model using isogeometric elements and the nonlinear transient formulation for plates is formed in the total Lagrange approach based on the von Kármán strains and solved by Newmark time integration. Through the thickness of each piezoelectric layer, the electric potential is assumed linearly. For active control of the piezoelectric composite plates, a close-loop system is used. An optimization procedure using genetic algorithm (GA) is considered to search optimal design for actuator input voltages. Various numerical examples are investigated to show high accuracy and reliability of the proposed method.

Keywords: Nonlinear transient response, Piezoelectric composite plates, Unconstrained theory, Isogeometric analysis (IGA), Sensors and actuators, Active control.

[*]Corresponding author: Email: hung.nx@vgu.edu.vn

1. Introduction

Piezoelectric materials belong to a smart material class that expresses electromechanical coupling. The development of smart structures integrated with sensors and actuators offers a considerable interest in many engineering applications: structural health monitoring, automotive sensors, actuators, vibration and noise suppression, shape control and precision positioning, etc. The main feature of smart materials is transformation between mechanical energy and electric energy. When the application of electric field to piezoelectric structures is considered, the mechanical deformation is generated. This is known as the converse phenomenon of piezoelectric effect [1,2].

With the advantages of piezoelectric materials, various numerical methods have been devised. Mitchell and Reddy [3] presented the classical plate theory (CPT) using the third order shear deformation theory (TSDT) to obtain the Navier solution for composite laminates with piezoelectric lamina. Suleman and Venkayya [4] used the classical laminate theory (CLT) with four-node finite element to investigate static and vibration analyses of a laminated composite with piezoelectric layer based on hourglass stabilization and reduced numerical integration Victor et al. [5] developed the higher order finite formulations based on an analytical solution to investigate the mechanics of composite structures integrated with actuators and sensors. Liew et al. [6] studied post-bucking of FGM plates integrated with piezoelectric under thermo-electro-mechanical loadings using a semi-analytical solution with Galerkin differential quadrature integration algorithm based on the higher-order shear deformation theory (HSDT). The radial point interpolation method (RPIM) combined with the first order shear deformation theory (FSDT) and the CPT with rectangular plate bending element were investigated by Liu et al. [7,8] to compute and simulate the static deformation and responses of smart plates. In addition, Hwang and Park [9] studied piezoelectric plates using the discrete Kirchhoff quadrilateral (DKQ) element and the Newmark β -method to analyze the direct time responses of the plate subjected to negative velocity feedback control. A HSDT-layerwise generalized finite element formulation [10] and the layerwise based on analytical formulation [11] were investigated to study piezoelectric composite plates. Finite element (FE) formulations based on HSDT for analysis of smart laminated plates was studied in [12]. Ray and Mallik [13] used FEM to study smart structures containing piezoelectric fiber-reinforced composite actuator. Nonlinear analysis for composite structures using some finite element methods (FEMs) were reported in Refs. [14-16]. It was proved in [17] that free vibration analysis using FEM leads to less accurate solution for high

frequencies. Such shortcomings become more challenges in coupled-field problems as piezoelectric structures.

For vibration control, Bailey et al. [18] and Shen et al. [19] investigated smart beams integrated with layers using analytical solutions. Tzou and Tseng [20] used a thin hexahedron solid element to examine dynamic control of piezoelectric plates and shells. The meshfree model based on FSDT was presented by Liew et al. [21] to simulate shape control of piezoelectric composite plates with different boundary conditions. Wang et al. [22] used FEM to investigate dynamic stability of piezoelectric composite plates, where the governing equations of motion using Lyapunov's energy [23] with active damping was used. Active control of geometrically nonlinear of composite structures was examined in Refs. [24,25]. Recently, isogeometric analysis (IGA) has been developed to investigate the piezoelectric composite plates by Phung-Van et al. [26]. However, nonlinear transient analysis has not considered in their previous work.

For optimal control, Kumar et al. [27] and Rao et al. [28] used GA to study the optimization problems for finding optimal piezo location on a cantilever plate and a two-bay truss. Chang-Qing et al. [29] investigated optimal control of piezoelectric structures using independent modal space control (IMSC). Optimal location of piezoelectric using GA for vibration control of structures was investigated by Bruant et al. [30]. In their work, two variables for each piezo-electric device in an optimization problem, the location of its center and its orientation, are considered. A closed-form solution based on the linear quadratic regulators (LQR) for the optimal control of piezoelectric composite plates was reported in [31].

It is known that FSDT requires the shear correction factors to ensure stability of solutions, but high accuracy of stresses is not guaranteed. HSDTs have then been developed to overcome the shortcomings of FSDT without any shear correction factors. Among HSDTs, the unconstrained third order shear deformation theory (UTSDT) [32] showed an alternative and effective approach for laminated plate structures. In addition, UTSDT allows us to relax traction-free boundary condition at the bottom and the top surfaces of plates, which is commonly required in HSDTs. The appearence of the unconstrained theory opens future applications of the UTSDT to the problems considering flow field in which the boundary layer of stresses is significant. The differential equations for UTSDT are of similar complexity to those of TSDT. This approach produces more accurate solutions [33]. Responses of the laminated plates using UTSDT were also investigated in [33]. Static and free vibration analyses of composite plates using radial point interpolation method (RPIM) combined with UTSDT were

reported in [34]. In UTSDT, the displacement field includes seven displacement components. More importantly, we here propose a generalized unconstrained HSDT that also uses seven displacement components like UTSDT, but higher order rotations depend on an arbitrary function $f(z)$ through the plate thickness.

Hughes et al. [35,36] developed isogeometric analysis (IGA) with the original objective of integrating Computer Aided Design (CAD) and FE analysis. The basic functions of IGA are the same with those of CAD (most notably NURBS or T-Splines). One of features of IGA is that it can easily achieve any desired degree of basic functions through the choice of the interpolation order, as opposed to traditional FEM where C^0 inter-element continuity is normally achieved. In the past few years, IGA has been successfully applied to various fields. Particular relevancy to this paper is the study of structural vibrations and the development of shell and plate isogeometric elements [37-45]. So far, there are few papers related to nonlinear analysis using IGA for composite plates based on FSDT [46,47], Euler–Bernoulli beams [48], shells [49] and so on. Apparently, there are no researches on geometrically nonlinear transient based on isogeometric analysis for the piezoelectric composite plates. Hence, we propose an efficient approach to fill this research gap via a generalized UHSDT and IGA. For reference, it is termed as IGA-UHSDT. The method will be applied for active control of geometrically nonlinear transient responses and optimization of smart piezoelectric composite plate structures. The IGA-UHSDT is used to approximate the displacement field of smart plates. Through the thickness of each piezoelectric layer, the electric potential is assumed linearly. The nonlinear transient formulation for plates is formed in the total Lagrange approach based on the von Kármán strains and solved by Newmark time integration. An optimization procedure based on GA is considered to find optimal input voltages. The reliability and accuracy of the method are confirmed by numerical examples.

2. A brief of NURBS basis functions

A knot vector $\Xi = \{\xi_1, \xi_2, ..., \xi_{n+p+1}\}$ is defined by a sequence of parameter values $\xi_i \in \mathbb{R}$, $i = 1, ..., n+p$. The knot vector is called open knot if the first and the last knots are repeated p+1 times. A B-spline basis function is C^{∞} continuous inside a knot span and C^{p-1} continuous at a single knot. The associated B-spline basis functions are defined recursively starting with the zeroth order basis function (p = 0) and a polynomial order $p \geq 1$,

$$N_{i,p}(\xi)=\frac{\xi-\xi_i}{\xi_{i+p}-\xi_i}N_{i,p-1}(\xi)+\frac{\xi_{i+p+1}-\xi}{\xi_{i+p+1}-\xi_{i+1}}N_{i+1,p-1}(\xi)$$
$$\text{as } p=0,\ N_{i,0}(\xi)=\begin{cases}1 & if \quad \xi_i\le\xi<\xi_{i+1}\\ 0 & \text{otherwise}\end{cases} \tag{1}$$

From the tensor product of basis functions with two knot vectors $\mathbf{H}=\{\eta_1,\eta_2,...,\eta_{m+q+1}\}$ and $\mathbf{\Xi}=\{\xi_1,\xi_2,...,\xi_{n+p+1}\}$ the B-spline basis functions can be obtained as

$$N_A(\xi,\eta)=N_{i,p}(\xi)M_{j,q}(\eta) \tag{2}$$

Figure 1 plots two sets of univariate quadratic and cubic B-splines, $\mathbf{\Xi}=\{0,0,0,\frac{1}{5},\frac{2}{5},\frac{3}{5},\frac{3}{5},\frac{4}{5},1,1,1\}$ and $\mathbf{H}=\{0,0,0,0,\frac{1}{4},\frac{1}{2},\frac{3}{4},1,1,1,1\}$, respectively.

Furthermore, the NURBS functions are expressed by adding an individual weight ζ_A. A NURBS functions are defined by their order, a set of weighted control points, and a knot vector. NURBS functions represent exactly circles, spheres, conic, cylinders sections. They have most of the properties of B-splines and can be expressed as

$$R_A(\xi,\eta)=\frac{N_A(\xi,\eta)\zeta_A}{\sum_{A=1}^{m\times n}N_A(\xi,\eta)\zeta_A} \tag{3}$$

Of course, the B-spline basis function is a special case of NURBS one.

3. Theory and formulation of piezoelectricity

A piezoelectric composite plate is considered and illustrated in Figure 2. Lower and upper layers of the composite plate are piezoelectric layers. The UHSDT is used to approximate the variable displacements for the composite plate, while the electrical displacements are assumed to be independent.

3.1 UHSDT

The unconstrained theory based on HSDT can be rewritten in a general form using an arbitrary function *f*(*z*) as follows

$$\begin{aligned}u(x,y,z,t)&=u_0(x,y,t)+zu_1(x,y,t)+f(z)u_2(x,y,t)\\ v(x,y,z,t)&=v_0(x,y,t)+zv_1(x,y,t)+f(z)v_2(x,y,t)\\ w(x,y,z,t)&=w(x,y,t)\end{aligned} \tag{4}$$

where u_0, u_1, u_2, v_0, v_1, v_2 and w are displacement variables; x, y, z are components of the Cartesian coordinate system $Oxyz$ and t is the time. For UTSDT in Ref. [32], the function $f(z) = z^3$ is used. Generally speaking, $f(z)$ can be defined as a continuous function such that its first derivative is nonlinear through the plate thickness. Moreover, there exists an optimal function $f_{op}(z)$ yielding best accurate solutions. However, the finding of $f_{op}(z)$ remains an open question. In what follows, we introduce a new function $f(z) = arctan(z)$ that ensures that its first derivative is nonlinear through the plate thickness and solutions are more accurate than for the case of $f(z) = z^3$.

For a plate bending, the strain vector is presented by

$$\varepsilon_{ij} = \frac{1}{2}\left(\frac{\partial u_i}{\partial x_j} + \frac{\partial u_j}{\partial x_i}\right) + \frac{1}{2}\frac{\partial u_k}{\partial x_i}\frac{\partial u_k}{\partial x_j} \tag{5}$$

Following the Von Karman theory, Eq. (5) can be rewritten as

$$\begin{aligned} \boldsymbol{\varepsilon}_p &= \boldsymbol{\varepsilon}_m + z\boldsymbol{\varepsilon}_1 + f(z)\boldsymbol{\varepsilon}_2 \\ \boldsymbol{\varepsilon}^s &= \boldsymbol{\varepsilon}_0^s + f'(z)\boldsymbol{\varepsilon}_1^s \end{aligned} \tag{6}$$

where

$$\begin{aligned} &\boldsymbol{\varepsilon}_m = \begin{bmatrix} u_{0,x} \\ v_{0,y} \\ u_{0,y} + v_{0,x} \end{bmatrix} + \frac{1}{2}\begin{bmatrix} w_{,x}^2 \\ w_{,y}^2 \\ 2w_{,xy} \end{bmatrix} = \boldsymbol{\varepsilon}_L + \boldsymbol{\varepsilon}_{NL}, \quad \boldsymbol{\varepsilon}_1 = \begin{bmatrix} u_{1,x} \\ v_{1,y} \\ u_{1,y} + v_{1,x} \end{bmatrix}, \quad \boldsymbol{\varepsilon}_2 = \begin{bmatrix} u_{2,x} \\ v_{2,y} \\ u_{2,y} + v_{2,x} \end{bmatrix}, \\ &\boldsymbol{\varepsilon}_0^s = \begin{bmatrix} u_1 + w_{,x} \\ v_1 + w_{,y} \end{bmatrix}, \quad \boldsymbol{\varepsilon}_1^s = \begin{bmatrix} u_2 \\ v_2 \end{bmatrix} \end{aligned} \tag{7}$$

in which the nonlinear component is computed as

$$\boldsymbol{\varepsilon}_{NL} = \frac{1}{2}\begin{bmatrix} w_{,x} & 0 \\ 0 & w_{,y} \\ w_{,y} & w_{,x} \end{bmatrix}\begin{Bmatrix} w_{,x} \\ w_{,y} \end{Bmatrix} = \frac{1}{2}\mathbf{A}_\theta\boldsymbol{\theta} \tag{8}$$

The material behaviour of smart composite plates is expressed as follows [50,51]

$$\begin{bmatrix} \boldsymbol{\sigma} \\ \mathbf{D} \end{bmatrix} = \begin{bmatrix} \mathbf{c} & -\mathbf{e}^T \\ \mathbf{e} & \mathbf{g} \end{bmatrix}\begin{bmatrix} \bar{\boldsymbol{\varepsilon}} \\ \mathbf{E} \end{bmatrix} \tag{9}$$

where $\bar{\boldsymbol{\varepsilon}} = [\boldsymbol{\varepsilon}_p \ \ \boldsymbol{\varepsilon}_s]^T$ and $\boldsymbol{\sigma}$ are the strain vector and the stress vector, respectively; $\mathbf{g}$ denotes the dielectric constant matrix and $\mathbf{D}$ is the dielectric displacement; $\mathbf{e}$ is the piezoelectric constant; $\mathbf{E}$, the electric field vector, can be defined as

$$\mathbf{E} = -\text{grad}\,\phi \tag{10}$$

in which ϕ is the electric potential field; and $\mathbf{c}$, the elasticity matrix, is defined as

$$\mathbf{c}=\begin{bmatrix}\mathbf{A} & \mathbf{B} & \mathbf{L} & \mathbf{0} & \mathbf{0}\\ \mathbf{B} & \mathbf{G} & \mathbf{F} & \mathbf{0} & \mathbf{0}\\ \mathbf{L} & \mathbf{F} & \mathbf{H} & \mathbf{0} & \mathbf{0}\\ \mathbf{0} & \mathbf{0} & \mathbf{0} & \mathbf{A}_s & \mathbf{B}_s\\ \mathbf{0} & \mathbf{0} & \mathbf{0} & \mathbf{B}_s & \mathbf{D}_s\end{bmatrix} \tag{11}$$

in which

$$\begin{aligned}(\mathbf{A},\mathbf{B},\mathbf{G},\mathbf{L},\mathbf{F},\mathbf{H})&=\int_{-h/2}^{h/2}\left(1,z,z^2,f(z),zf(z),f^2(z)\right)\bar{Q}_{ij}\mathrm{d}z \qquad i,j=1,2,6\\ (\mathbf{A}_s,\mathbf{B}_s,\mathbf{D}_s)&=\int_{-h/2}^{h/2}\left(1,f'(z),\left(f'(z)\right)^2\right)\bar{Q}_{ij}\mathrm{d}z \qquad i,j=4,5\end{aligned} \tag{12}$$

where $\bar{Q}_{ij}$ is calculated as in [52].

3.2 Approximation of mechanical displacements and electric potential field

3.2.1 Mechanical displacements

Using NURBS basic function, the field **u** of the composite plate is approximated as

$$\mathbf{u}^h(\xi,\eta)=\sum_{I=1}^{m\times n}N_I(\xi,\eta)\mathbf{d}_I \tag{13}$$

where $\mathbf{d}_I=\begin{bmatrix}u_{0I} & v_{0I} & u_{1I} & v_{1I} & u_{2I} & v_{2I} & w_I\end{bmatrix}^T$, and N_I is the shape function as defined in Section 2.

Substituting Eq. (13) into Eqs. (6)-(8), the strains can be rewritten as

$$\bar{\boldsymbol{\varepsilon}}=[\boldsymbol{\varepsilon}_p \;\; \boldsymbol{\varepsilon}_s]^T=\sum_{I=1}^{m\times n}\left(\mathbf{B}_I^L+\frac{1}{2}\mathbf{B}_I^{NL}\right)\mathbf{d}_I \tag{14}$$

where $\mathbf{B}_I^L=\begin{bmatrix}\mathbf{B}_I^0 & \mathbf{B}_I^1 & \mathbf{B}_I^2 & \mathbf{B}_I^{s0} & \mathbf{B}_I^{s1}\end{bmatrix}^T$, in which

$$\begin{aligned}\mathbf{B}_I^0&=\begin{bmatrix}N_{I,x} & 0 & 0 & 0\,0\,0\,0\\ 0 & N_{I,y} & 0 & 0\,0\,0\,0\\ N_{I,y} & N_{I,x} & 0 & 0\,0\,0\,0\end{bmatrix},\ \mathbf{B}_I^1=\begin{bmatrix}0 & 0 & N_{I,x} & 0 & 0\,0\,0\\ 0 & 0 & 0 & N_{I,y} & 0\,0\,0\\ 0 & 0 & N_{I,y} & N_{I,x} & 0\,0\,0\end{bmatrix},\\ \mathbf{B}_I^2&=\begin{bmatrix}0\,0\,0 & 0 & N_{I,x} & 0 & 0\\ 0\,0\,0 & 0 & 0 & N_{I,y} & 0\\ 0\,0\,0 & 0 & N_{I,y} & N_{I,x} & 0\end{bmatrix},\\ \mathbf{B}_I^{s0}&=\begin{bmatrix}0 & 0 & N_I & 0 & 0\,0\,N_{I,x}\\ 0 & 0 & 0 & N_I & 0\,0\,N_{I,y}\end{bmatrix},\ \mathbf{B}_I^{s1}=\begin{bmatrix}0\,0 & 0\,0 & N_I & 0 & 0\\ 0\,0 & 0\,0 & 0 & N_I & 0\end{bmatrix}\end{aligned} \tag{15}$$

and $\mathbf{B}_I^{NL}$ is calculated by

$$\mathbf{B}_I^{NL}(\mathbf{d})=\begin{bmatrix}w_{I,x} & 0\\ 0 & w_{I,y}\\ w_{I,y} & w_{I,x}\end{bmatrix}\begin{bmatrix}0\,0\,0\,0\,0\,0\,N_{I,x}\\ 0\,0\,0\,0\,0\,0\,N_{I,x}\end{bmatrix}=\mathbf{A}_\theta\mathbf{B}_I^g \tag{16}$$

3.2.2 Electric potential field

The electric potential field is approximated as follows [54]

$$\phi^i(z) = \mathbf{N}_\phi^i \boldsymbol{\phi}^i \tag{17}$$

where $\mathbf{N}_\phi^i$ is the shape functions defined in section 2 with $p = 1$, and $\boldsymbol{\phi}^i = \begin{bmatrix} \phi^{i-1} & \phi^i \end{bmatrix}$ $(i = 1, 2, ..., n_{sub})$ in which n_{sub} is the number of piezoelectric layers.

In each piezoelectric element, electric potentials are assumed to be equal at height along the thickness [51,53]. The **E** in Eq. (10) is rewritten

$$\mathbf{E} = -\nabla \mathbf{N}_\phi^i \boldsymbol{\phi}^i = -\mathbf{B}_\phi \boldsymbol{\phi}^i \tag{18}$$

Note that, for the type of piezoelectric materials considered in this work **e** and **g** of the k^{th} layer in the local coordinate system can be written as follows [54]

$$\mathbf{e}^{(k)} = \begin{bmatrix} 0 & 0 & 0 & 0 & d_{15} & 0 \\ 0 & 0 & 0 & d_{15} & 0 & 0 \\ d_{31} & d_{32} & d_{33} & 0 & 0 & 0 \end{bmatrix}^{(k)} \quad ; \quad \mathbf{g}^{(k)} = \begin{bmatrix} p_{11} & 0 & 0 \\ 0 & p_{22} & 0 \\ 0 & 0 & p_{33} \end{bmatrix}^{(k)} \tag{19}$$

The piezoelectric constant matrix for the k^{th} layer in the global coordinate system is given by

$$\mathbf{e}^{(k)} = \begin{bmatrix} 0 & 0 & 0 & 0 & \overline{d}_{15} & 0 \\ 0 & 0 & 0 & \overline{d}_{15} & 0 & 0 \\ \overline{d}_{31} & \overline{d}_{32} & \overline{d}_{33} & 0 & 0 & 0 \end{bmatrix}^{(k)} \quad ; \quad \mathbf{g}^{(k)} = \begin{bmatrix} \overline{p}_{11} & 0 & 0 \\ 0 & \overline{p}_{22} & 0 \\ 0 & 0 & \overline{p}_{33} \end{bmatrix}^{(k)} \tag{20}$$

where $\overline{d}_{ij}$ and $\overline{p}_{ii}$ are calculated similar to $\overline{Q}_{ij}$ in Eq. (12).

3.3 Governing equations

The equations for the smart plate are written

$$\begin{bmatrix} \mathbf{M}_{uu} & 0 \\ 0 & 0 \end{bmatrix} \begin{bmatrix} \ddot{\mathbf{d}} \\ \ddot{\boldsymbol{\phi}} \end{bmatrix} + \begin{bmatrix} \mathbf{K}_{uu} & \mathbf{K}_{u\phi} \\ \mathbf{K}_{\phi u} & \mathbf{K}_{\phi\phi} \end{bmatrix} \begin{bmatrix} \mathbf{d} \\ \boldsymbol{\phi} \end{bmatrix} = \begin{bmatrix} \mathbf{f} \\ \mathbf{Q} \end{bmatrix} \quad \Leftrightarrow \quad \overline{\mathbf{M}}\ddot{\mathbf{q}} + \overline{\mathbf{K}}\mathbf{q} = \overline{\mathbf{f}} \tag{21}$$

where

$$\begin{aligned} &\mathbf{K}_{uu} = \int_\Omega (\mathbf{B}^L + \mathbf{B}^{NL})^T \mathbf{c} (\mathbf{B}^L + \tfrac{1}{2}\mathbf{B}^{NL}) \mathrm{d}\Omega \quad ; \quad \mathbf{K}_{u\phi} = \int_\Omega (\mathbf{B}^L)^T \mathbf{e}^T \mathbf{B}_\phi \mathrm{d}\Omega \\ &\mathbf{K}_{\phi\phi} = \int_\Omega \mathbf{B}_\phi^T \mathbf{p} \mathbf{B}_\phi \mathrm{d}\Omega \quad ; \quad \mathbf{M}_{uu} = \int_\Omega \tilde{\mathbf{N}}^T \mathbf{m} \tilde{\mathbf{N}} \mathrm{d}\Omega \quad ; \quad \mathbf{f} = \int_\Omega \overline{q}_0 \overline{\mathbf{N}} \mathrm{d}\Omega \end{aligned} \tag{22}$$

in which q_0 is a uniform load; $\overline{\mathbf{N}} = \begin{bmatrix} 0 & 0 & 0 & 0 & 0 & 0 & N_I \end{bmatrix}$; **m** is defined by

$$\mathbf{m} = \begin{bmatrix} I_1 & I_2 & I_4 \\ I_2 & I_3 & I_5 \\ I_4 & I_5 & I_7 \end{bmatrix}, \quad (I_1, I_2, I_3, I_4, I_5, I_7) = \int_{-h/2}^{h/2} \rho \left(1, z, z^2, f(z), zf(z), f^2(z)\right) \mathrm{d}z \tag{23}$$

and

$$\tilde{\mathbf{N}}=\begin{Bmatrix}\mathbf{N}_1\\ \mathbf{N}_2\\ \mathbf{N}_3\end{Bmatrix},\ \mathbf{N}_1=\begin{bmatrix}N_I & 0 & 0\,0 & 0\,0 & 0\\ 0 & N_I & 0\,0 & 0\,0 & 0\\ 0 & 0 & 0\,0 & 0\,0 & N_I\end{bmatrix},$$
$$\mathbf{N}_2=\begin{bmatrix}0 & 0 & N_I & 0 & 0\,0\,0\\ 0 & 0 & 0 & N_I & 0\,0\,0\\ 0 & 0 & 0 & 0 & 0\,0\,0\end{bmatrix},\ \mathbf{N}_3=\begin{bmatrix}0 & 0\,0 & 0\,0 & N_I & 0\\ 0 & 0\,0 & 0\,0 & 0 & N_I\\ 0 & 0\,0 & 0\,0 & 0 & 0\end{bmatrix} \tag{24}$$

Substituting the second row of Eq. (21) into the first row, Eq. (21) can be expressed as

$$\mathbf{M}\ddot{\mathbf{d}}+\left(\mathbf{K}_{uu}+\mathbf{K}_{u\phi}\mathbf{K}_{\phi\phi}^{-1}\mathbf{K}_{\phi u}\right)\mathbf{d}=\mathbf{F}+\mathbf{K}_{u\phi}\mathbf{K}_{\phi\phi}^{-1}\mathbf{Q} \tag{25}$$

4. Active control analysis

We now consider a composite plate integrated piezoelectric with *n (n ≥ 2)* layers as shown in Figure 13. The sensor layer (the bottom layer) is denoted with the subscript *s* and the charge Q is considered to be zero. Using the second row of Eq. (21), the sensor output can be expressed by

$$\boldsymbol{\phi}_s=\left[\mathbf{K}_{\phi\phi}^{-1}\right]_s\left[\mathbf{K}_{\phi u}\right]_s\mathbf{d}_s \tag{26}$$

where G_d and G_v are the constant gains of the displacement feedback control and velocity feedback control, respectively.

The control law on the actuator layer, labeled with the subscript *a,* can be defined by [7]

$$\boldsymbol{\phi}_a=G_d\boldsymbol{\phi}_s+G_v\dot{\boldsymbol{\phi}}_s \tag{27}$$

Substituting Eqs. (26)-(27) into Eq. (21), we obtain

$$\mathbf{Q}_a=\left[\mathbf{K}_{uu}\right]_a\mathbf{d}_a-G_d\left[\mathbf{K}_{\phi\phi}\right]_a\left[\mathbf{K}_{\phi\phi}^{-1}\right]_s\left[\mathbf{K}_{\phi u}\right]_s\mathbf{d}_s-G_v\left[\mathbf{K}_{\phi\phi}\right]_a\left[\mathbf{K}_{\phi\phi}^{-1}\right]_s\left[\mathbf{K}_{\phi u}\right]_s\dot{\mathbf{d}}_s \tag{28}$$

Substituting Eqs. (26) and (28) into Eq. (25), one writes

$$\mathbf{M}\ddot{\mathbf{d}}+\mathbf{C}\dot{\mathbf{d}}+\mathbf{K}^*\mathbf{d}=\mathbf{F} \tag{29}$$

where

$$\mathbf{K}^*=\mathbf{K}_{uu}+G_d\left[\mathbf{K}_{u\phi}\right]_s\left[\mathbf{K}_{\phi\phi}^{-1}\right]_s\left[\mathbf{K}_{\phi u}\right]_s \tag{30}$$

and the active damping matrix, **C**, can be computed by

$$\mathbf{C}=G_v\left[\mathbf{K}_{u\phi}\right]_a\left[\mathbf{K}_{\phi\phi}^{-1}\right]_s\left[\mathbf{K}_{\phi u}\right]_s \tag{31}$$

Without effect of the structural damping, Eq. (29) can be rewritten as

$$\mathbf{M}\ddot{\mathbf{d}}+\mathbf{K}^*\mathbf{d}=\mathbf{F} \tag{32}$$

For static analyses, Eq. (29) reduces to

$$\mathbf{K}^*\mathbf{d}=\mathbf{F} \tag{33}$$

5. Nonlinear transient analysis

The equation for nonlinear transient analysis shown in Eq. (21) is now considered. At initial time, $t = 0$, displacements, velocities and accelerations are zero. Based on the Newmark method [55], a new state,

i.e., the first and second derivative of displacements at $(m+1)\Delta t$, is found using the following formulations

$$\ddot{\mathbf{q}}_{m+1} = \frac{1}{\beta \Delta t^2}(\mathbf{q}_{m+1} - \mathbf{q}_m) - \frac{1}{\beta \Delta t}\dot{\mathbf{q}}_m - \left(\frac{1}{2\beta} - 1\right)\ddot{\mathbf{q}}_m \tag{34}$$

$$\dot{\mathbf{q}}_{m+1} = \dot{\mathbf{q}}_m + \Delta t(1-\gamma)\ddot{\mathbf{q}}_m + \gamma \Delta t \ddot{\mathbf{q}}_{m+1} \tag{35}$$

where $\beta = 0.25$ and $\gamma = 0.5$ as in Ref. [56].

Substituting Eq. (34) into Eq. (21), we obtain

$$\left(\bar{\mathbf{K}}_{m+1} + \frac{1}{\beta \Delta t^2}\bar{\mathbf{M}}\right)\mathbf{q}_{m+1} = \bar{\mathbf{f}}_{m+1} + \bar{\mathbf{M}}\left[\frac{1}{\beta \Delta t^2}\mathbf{q}_m + \frac{1}{\beta \Delta t}\dot{\mathbf{q}}_m + \left(\frac{1}{2\beta} - 1\right)\ddot{\mathbf{q}}_m\right] \tag{36}$$

To solve Eq. (36), the Newton-Raphson method [57] is used in this work and the residual force, $\boldsymbol{\varphi}$, is introduced to present errors of the approximation. During each iteration, $\boldsymbol{\varphi}$ needs to tend to zeros and can be defined at time step $(m+1)\Delta t$, $\boldsymbol{\varphi}_{m+1}$, as follows

$$\boldsymbol{\varphi}_{m+1} = \tilde{\mathbf{K}}_{m+1}\mathbf{q}_{m+1} - \tilde{\mathbf{f}}_{m+1} \tag{37}$$

To have unbalanced residual force, an improved solution, ${}^{i+1}\mathbf{q}_{m+1}$, can be updated

$${}^{i+1}\mathbf{q}_{m+1} = {}^{i}\mathbf{q}_{m+1} + \Delta\mathbf{q} \tag{38}$$

where ${}^{i}\mathbf{q}_{m+1}$ is an approximate trial solution at the i^{th} iteration and $\Delta\mathbf{q}$ is the incremental displacement and expressed by [58]

$$\Delta\mathbf{q} = -{}^{i}\boldsymbol{\varphi}_{m+1} / \mathbf{K}_T \tag{39}$$

in which $\mathbf{K}_T$ is tangent stiffness matrix

$$\mathbf{K}_T = \partial\boldsymbol{\varphi}({}^{i}\mathbf{q}) / \partial\mathbf{q} \tag{40}$$

At each time step, Eq. (38) is repeated until the error between two consecutive iterations is less then the tolerance error

$$\frac{\left\| {}^{i+1}\mathbf{q}_{m+1} - {}^{i}\mathbf{q}_{m+1} \right\|}{\left\| {}^{i}\mathbf{q}_{m+1} \right\|} < tol \tag{41}$$

6. Numerical validations

This section shows the performance of the method through various numerical examples. The following symbols for boundary conditions are used: free (F), simply supported (S) or clamped (C) edges. The symbol, SSSS, represents a rectangular plate with fully simply supported edges. In addition, Table 1

shows the properties of the piezoelectric composite plates, including Poisson's ration (ν), mass density (ρ), elastic properties (E), piezoelectric coefficients (d) and electric permittivities (p) and shear modulus (G). Note that the properties 1, 2 and 3 in Table 1 refer to the directions of axes x, y and z, respectively.

6.1 Free vibration and of smart plates

6.1.1 Static analysis

A square smart plate with length 20 cm under a uniform load q = 100 N/m^2 plotted in Figure 3 is considered. The plate has six layers: two outer piezo layers represented by *pie* and four composite layers. The configurations of the plate are $[pie/\text{-}\theta/\theta]_s$ and $[pie/\text{-}\theta/\theta]_{as}$ where "*as*" and "*s*" indicate anti-symmetric and symmetric, respectively; θ is the fiber orientation. Each layer thickness of the non-piezoelectric composite plate is 0.25 mm and the thickness of the piezo layer is 0.1 mm. The composite layers are made of T300/976 graphite/epoxy and the piezo-ceramic layers are PZTG1195N.

First, the effect of input voltages on deflection of the CFFF plate $[pie/\text{-}45/45]_{as}$ is shown in Figure 4. It can be seen, the present results agree well with those of Refs [7,59].

For the SSSS plate, different fiber orientation angles such as $[pie/\text{-}15/15]_{as}$, $[pie/\text{-}30/30]_{as}$, $[pie/\text{-}45/45]_{as}$ and $[pie/\text{-}45/45]_s$ are investigated.

Table 2 plots the deflection of the plate. It can be seen that the results of IGA-UHSDT match well

with those of Ref. [7]. In addition, the deflection of plate under different input voltages 0V, 5V, 8V, 10V is shown in Figure 5. The deflection decreases for increasing input voltage as expected. The reason is that the input voltage induces an upward deflection of the plate due to the piezoelectric effect. This upward contribution becomes prevalent for an input voltage of 10V. Similar results were obtained in Ref.[7]. Next, the centerline deflection of a plate with configurations $[-45/p/45]_{as}$ and $[-15/p/15]_{as}$ is plotted in Figure 6. Again, we can see that results in Figure 6a match well with those of RPIM in Ref. [7]. Also, as the fiber orientation angle decreases, the deflection of the plate increases.

Furthermore, the deflection of the plate using only mesh of 9×9 elements with different boundary conditions (CFFF, SSFF, SSSS) is shown in Figure 7. Again, it can be seen that the present method agrees very well with those of RPIM [7].

6.1.2 Free vibration analysis

In this section, the accuracy of isogeometric finite elements is investigated in case of free vibration of plates. A SSSS plate [*pie*/0/90/0/*pie*] (length *a*, thickness *t* and *t*/*a* = 1/50) is considered and shown in Figure 8. The composite layers are made of *Gp*/*Ep* and thickness of two PZT-4 piezoelectric layers is 0.1*t*. Two electric boundary conditions are investigated: (1) an open-circuit condition where the electric potential remains free; and (2) a closed-circuit condition in which the electric potential is kept zero (grounded). The analytical solution for the first natural frequency was studied by Heyliger and Saravanos [60]. Victor et al. [5] and Saravanos et al. [11] using finite element formulations were also reported to obtain different natural frequencies.

The dimensionless first natural frequency, $\bar{f} = \omega_1 a^2 / \left(1000t\sqrt{\rho}\right)$, is considered where ω_1 is the first natural frequency. Table 3 shows the dimensionless first natural frequency of the plate with three types of elements: quadratic (p = 2), cubic (p = 3) and quartic (p = 4). The results given by the IGA-UHSDT formulation are slightly lower than the analytical solution [60]. Besides, we can see that the results of the present method are stable in both closed-circuit condition and open-circuit condition similarly to the analytical solution in [60], while those of Refs. [5,11] are slightly deviated. This was also addressed in [61] to show the better performance of IGA over the conventional FEM in the solution of eigenvalue problems. In addition,

Table 4 shows the convergence of the first five natural frequencies. Again, it can be seen that the IGA-UHSDT results match well with those of Refs. [5,11,60] and are stable for both closed- and open-circuit conditions. Figure 9 shows shapes of six eigenmodes. We can see that these shapes reflect correctly physical modes of the piezoelectric composite plates as given by the analytical solution.

Next, a square six-ply plate $[pie/\text{-}45/45]_{as}$ is considered. The length of plate is 20 cm and thickness of the non-piezoelectric composite plate is 1 mm and each layer has the same thickness. The thickness of the piezo-layer is 0.1 mm. The plate is made of T300/976 graphite/epoxy layers and the piezo-ceramic is PZTG1195N. Table 5 shows the first ten natural frequencies of the plate using mesh of 13×13 B-spline elements with boundary conditions: CFFF and SSSS. It is again confirmed that the results of the present method match well with those of Refs. [7,59].

6.2 Nonlinear analysis of piezoelectric composite plates

6.2.1 An orthortropic plate

In this section, a SSSS square plate under a uniform loading of q_0 = 1 MPa with an aim to verify the accuracy of the present method for geometrically nonlinear transient analysis is studied. Material properties and the geometry are considered as follows: Young's modulus E_1 = 525 GPa, E_2 = 21 GPa, shear modulus $G_{12} = G_{23} = G_{13}$ = 10.5 GPa, Poisson's ratio v = 0.25, mass density ρ = 800 kg/m^3, length of the plate L = 250 mm, thickness h = 5 mm. Figure 10 shows the normalized central deflection, $\overline{w} = w / h$, of the plate. It can be seen that deflection responses of present method match well with those of finite strip method (FSM) [62].

6.2.2 Smart plates

Now consider a smart plate with material properties and geometrical dimensions are similar to section 6.1.1. For the plate under mechanical load (parameter load $\overline{q} = q_o \times 10^2$), Figure 11 shows the nonlinear deflection of the plate subjected to input voltages. We see that when voltage inputs increase, geometrically nonlinear deflection is upward. Moreover, the central deflection of the plate under input voltage 8V with different fiber orientation angles is shown in Figure 12.

6.3 Dynamic control and optimization

It is well known that structural controls play role advantages and benefits in the practice such as reduced energy consumption, improved product, increased safety, etc. The sentence, "control will be the physics of the 21st century", was spoken by Doyle JC (2001) at Conference on Decision and Control. As known, feedback and control are important in most technological aspects. In this work, we investigate behaviours of the plate under dynamic control.

6.3.1 Nonlinear transient vibration

We now consider a plate [*pie*/-45/45]$_s$ under a uniform load q = 100 N/m^2 that is similar to the plate in section 6.1.1. The upper and lower surfaces of plate are bonded to a piezoelectric actuator layer and a piezoelectric sensor layer, respectively. We first study the response of static control with meshing 9×9 and p = 2. The effect of the displacement feedback control gain G_d on the static deflection of the plate is shown in Figure 14. It is seen that when G_d increases, the deflections reduce, similarly to what reported in [7]. It is observed that as the plate is subjected to loadings, electric charges are generated and amplified through the control. Then, the signal is sent to the actuator and a voltage is generated. Through the converse effect of piezoelectric, a force is generated and actively controls the behavior of

the plate.

Next, a smart composite plate subjected to sinusoidally distributed transverse loads is investigated. The sinusoidally distributed transverse load is expressed as follows

$$q = q_0 \sin\left(\frac{\pi x}{L}\right)\sin\left(\frac{\pi y}{L}\right)F(t) \tag{42}$$

where

$$F(t) = \begin{cases} \begin{cases} 1 & 0 \le t \le t_1 \\ 0 & t > t_1 \end{cases} & \text{Step load} \\ \begin{cases} 1 - t/t_1 & 0 \le t \le t_1 \\ 0 & t > t_1 \end{cases} & \text{Triangular load} \\ -e^{-\gamma t} & \text{Explosive blast load} \end{cases} \tag{43}$$

in which q_0 = 4e8 Pa, γ = 330 s^{-1}. Figure 15 to Figure 17 show nonlinear transient vibrations of the central point of the plate under a closed-loop control. We observe that the response with control is smaller than those without control, as expected.

6.3.2 Optimization

Finally, we investigate optimization problems for actuator input voltages. Material properties and dimensions of piezoelectric plate are similar as in section 6.1. From Figure 4 and Figure 5, it can be seen that when the actuator input voltage increases, the deflection shape of plate is changed and upward. Here we can search an optimal voltage for piezoelectric plate with minimum energy. Figure 18 depicts the convergence of objective function using GA with 20 generations for the [*pie*/-45/45]$_{as}$ plate (SSSS) using a mesh of 9×9 cubic elements. Table 6 displays energy of plate with different actuator input voltages shown in Figure 4 and Figure 5 and the optimal input voltage. We can see that energy of plate for case optimal voltage V = 20.7 and 5.4 for CFFF and SSSS plates is minimum.

7. Conclusions

This paper presented a simple and effective approach based on the combination of IGA and a generalized unconstrained approach for dynamic control and optimization of smart piezoelectric composite plates. The new function through the plate thickness for the UHSDT was introduced, which can enhance the accuracy of the solution. The NURBS basis functions were used to handle any desired

degree of smoothness through the choice of the interpolation order and easily fulfills the C^1-continuity requirements for plate elements stemming from the HSDT. In static and free vibration analyses, the results of the present method are more accurate than those of several other methods with the lower number of degrees of freedom. The proposed approach is highly suitable for dynamic control under the nonlinear transient response. We believe that the present approach would provide a reliable source of reference when calculating smart piezoelectric composite plates with other methods.

Acknowledgements

The first and third authors would like to acknowledge the support from Erasmus Mundus Action 2, Lotus Unlimited Project.

The second author, Lieu B. Nguyen, thanks partial funding provided by University of Technical Education Ho Chi Minh City, Vietnam (Project No.: T2015-18TĐ).

References

[1] Z. Wang, S. Chen, W. Han, The static shape control for intelligent structures, Finite Elements in Analysis and Design 26 (1997) 303-314

[2] L. Costa , I. Figueiredo, R. Leal, P. Oliveira, G. Stadler, Modeling and numerical study of actuator and sensor effects for a laminated piezoelectric plate, Computers and Structures 85 (2007) 385-403

[3] J.A. Mitchell, J.N. Reddy, A refined hybrid plate theory for composite laminates with piezoelectric laminae, International Journal of Solids and Structures 32(16) (1995) 2345-2367

[4] A. Suleman, V.B. Venkayya, A simply finite element formulation for a laminated composite plate with piezoelectric layers, Journal of Intelligent Material Systems and Structures 6 (1995) 776-782

[5] M.F.C. Victor, A.A.G. Maria, S. Afzal, M.M.S. Cristóvão, A.M.S. Carlos, C.V.M. Franco, Modelling and design of adaptive composite structures, Computer Methods in Applied Mechanics and Engineering 185 (2000) 325-346

[6] K.M. Liew, J. Yang, S. Kittipornchai, Postbuckling of piezoelectric FGM plates subjected to thermo-electro-mechanical loading, International Journal of Solids and Structures 40 (2004) 3869-3892

[7] G.R. Liu, K.Y. Dai, K.M. Lim, Static and vibration control of composite laminates integrated with piezoelectric sensors and actuators using the radial point interpolation method, Smart Materials and Structures 13 (2004) 1438-1447.

[8] G.R. Liu, X.Q. Peng, K.Y. Lam, J. Tani, Vibration control simulation of laminated composite plates with integrated piezoelectrics, Journal of Sound and Vibration 220 (1999) 827–846

[9] W.C. Hwang, H.C. Park, Finite element modeling of piezoelectric sensors and actuators, AIAA

Journal 31 (1993) 930-937

[10] D.A.F. Torres, Pd.T.R Mendonca, C.S.D. Barcellos, Evaluation and verification of an HSDT-layerwise generalized finite element formulation for adaptive piezoelectric laminated plates, Computer Methods in Applied Mechanics and Engineering 200 (2011) 675-691

[11] D.A. Saravanos, P.R. Heyliger, D.A. Hopkins, Layerwise mechanics and finite element for the dynamic analysis of piezoelectric composite plates, International Journal of Solids and Structures 34 (1997) 359-378

[12] J.N. Reddy, On laminated composite plates with integrated sensors and actuators, Engineering Structures 21 (1999) 568–593

[13] M.C. Ray, N. Mallik, Finite element analysis of smart structures containing piezoelectric fiber-reinforced composite actuator, AIAA journal 42 (7) (2004) 1398-1405

[14] Loc V. Tran, Jaehong Lee, H. Nguyen-Van, H. Nguyen-Xuan, M.A. Wahab, Geometrically nonlinear isogeometric analysis of laminated composite plates based on higher-order shear deformation theory, International Journal of Non-Linear Mechanics 72 (2015) 42-52

[15] P. Phung-Van, T. Nguyen-Thoi, T. Bui-Xuan, Q. Lieu-Xuan, A cell-based smoothed three-node Mindlin plate element (CS-FEM-MIN3) based on the C0-type higher-order shear deformation for geometrically nonlinear analysis of laminated composite plates, Computational Materials Science 96 (2015) 549-558

[16] P. Phung-Van, .T Nguyen-Thoi, H. Luong-Van, Q. Lieu-Xuan, Geometrically nonlinear analysis of functionally graded plates using a cell-based smoothed three-node plate element (CS-MIN3) based on the C0-HSDT, Computer Methods in Applied Mechanics and Engineering 270 (2014) 15-36

[17] J.A. Cottrell, A. Reali, Y. Bazilevs, T.J.R. Hughes, Isogeometric analysis of structural vibrations, Computer Methods in Applied Mechanics and Engineering 195(41-43) (2006) 5257–5296

[18] T. Bailey, J.E. Hubbard, Distributed piezoelectric-polymer active control of a cantilever beam, Journal of Guidance Control and Dynamic 8 (1985) 605–611.

[19] I.S. Shen, Bending and torsional vibration control of composite beams through intelligent constrained-layer damping treatments, Smart Materials and Structures 4 (1995) 340–355

[20] H.S. Tzou, C.I. Tseng, Distributed piezoelectric sensor/actuation design for dynamic measurement/control of distributed systems: a piezoelectric finite element approach, Journal of Sound and Vibration 138 (1990) 17-34

[21] K.M. Liew, H.K. Lim, M.J. Tan, X.Q. He, Analysis of laminated composite beams and plate with piezoelectric patches using the element-free Galerkin method, Computational Mechanics 29 (2002) 486-497

[22] S.Y. Wang, S.T. Quek, K.K. Ang, Dynamic stability analysis of finite element modeling of piezoelectric composite plates, International Journal of Solids and Structures 41 (2004) 745-764

[23] A.M. Lyapunov, The general problem of the stability of motion, Taylor and Francis, 1992

[24] S. Panda, M.C. Ray, Active control of geometrically nonlinear vibrations of functionally graded laminated composite plates using piezoelectric fiber reinforced composites, Journal of Sound and Vibration 325(1) (2009) 186-205

[25] S.K. Sarangi, M.C. Ray, Active damping of geometrically nonlinear vibrations of doubly curved laminated composite shells, Composite Structures 93(12) (2011) 3216-3228

[26] P. Phung-Van, L. De Lorenzis, Chien H. Thai, M. Abdel-Wahab, H. Nguyen-Xuan, Analysis of laminated composite plates integrated with piezoelectric sensors and actuators using higher-order shear deformation theory and isogeometric finite elements, Computational Materials Science 96 (2015) 496-505

[27] R.K. Kumar, S. Narayanan, Active vibration control of beams with optimal placement of piezoelectric sensor/actuator pairs, Smart Materials and Structures 17 (2008) 055008

[28] S.S. Rao, T. Shii Pan, Optimal placement of actuators in actively controlled structures using genetic algorithms, AIAA Journal 29 (1991) 942–943

[29] C. Chang-Qing, S. Ya-Peng, Optimal control of active structures with piezoelectric modal sensors and actuators, Smart Materials and Structures 6 (1997) 403-409

[30] I. Bruant, L. Gallimard, S. Nikoukar, Optimal piezoelectric actuator and sensor location for active vibration control, using genetic algorithm, Journal of Sound and Vibration 329 (2010) 1615–1635

[31] M.C. Ray, Optimal Control of Laminated Plate with Piezoelectric Sensor and Actuator Layers, AIAA Journal 36(12) (1998) 2204-2208

[32] A.Y.T. Leung, An unconstrained third-order plate theory, Composite Structures 40(4) (1991) 871–875

[33] A.Y.T. Leung, N. Junchuan, C.W. Lim, S. Kongjie, A new unconstrained third- order plate theory for Navier solutions of symmetrically laminated plates, Computers and Structures 81 (2003) 2539–2548

[34] L.M.J.S. Dinis, R.M. Natal Jorge, J. Belinha, Static and dynamic analysis of laminated plates based on an unconstrained third order theory and using a radial point interpolator meshless method, Computers and Structures 89 (2011) 1771–1784

[35] T.J.R. Hughes, J.A. Cottrell, Y. Bazilevs, Isogeometric analysis: CAD, finite elements, NURBS, exact geometry and mesh refinement, Computer Methods in Applied Mechanics and Engineering 194(39-41) (2005) 4135–4195

[36] J.A. Cottrell, T.J.R. Hughes, Y. Bazilevs, Isogeometric Analysis, Towards Integration of CAD and FEA, Wiley, 2009

[37] D.J. Benson, Y. Bazilevs, M.C. Hsu, T.J.R. Hughes, Isogeometric shell analysis: The Reissner–Mindlin shell, Computer Methods in Applied Mechanics and Engineering 199(5-8) (2006) 276–289.

[38] P. Phung-Van, M. Abdel-Wahab, K.M. Liew, S.P.A. Bordas, H. Nguyen-Xuan, Isogeometric analysis of functionally graded carbon nanotube-reinforced composite plates using higher-order shear deformation theory, Composite Structures 123 (2015) 137-149

[39] H. Nguyen-Xuan, Loc V. Tran, Chien H. Thai, S. Kulasegaram, S.P.A. Bordas, Isogeometric analysis of functionally graded plates using a refined plate theory, Composites Part B: Engineering 64 (2014) 222-234

[40] V.P. Nguyen, P. Kerfriden, S.P.A. Bordas, T. Rabczuk, Isogeometric analysis suitable trivariate

NURBS representation of composite panels with a new offset algorithm, Computer Aided Design 55 (2014) 49-63

[41] Chien H. Thai, H. Nguyen-Xuan, N. Nguyen-Thanh, T.H. Le, T. Nguyen-Thoi, T. Rabczuk, Static, free vibration, and buckling analysis of laminated composite Reissner–Mindlin plates using NURBS-based isogeometric approach, International Journal for Numerical Methods in Engineering 91(6) (2012) 571–603

[42] Chien H. Thai, A.J.M Ferreira, S.P.A. Bordas, T. Rabczuk, H. Nguyen-Xuan, Isogeometric analysis of laminated composite and sandwich plates using a new inverse trigonometric shear deformation theory, European Journal of Mechanics - A/Solids 43 (2014) 89 - 108

[43] V.P. Nguyen, H. Nguyen-Xuan, High-order B-splines based finite elements for delamination analysis of laminated composites, Composite Structures 102 (2013) 261-275

[44] Loc V. Tran, Chien H. Thai, H. Nguyen-Xuan, An isogeometric finite element formulation for thermal buckling analysis of functionally graded plates, Finite Element in Analysis and Design 73 (2013) 65-76.

[45] N. Nguyen-Thanh, J. Kiendl, H. Nguyen-Xuan, R. Wüchner, K.U. Bletzinger, Y. Bazilevs, T. Rabczuk, Rotation free isogeometric thin shell analysis using PHT-splines, Computer Methods in Applied Mechanics and Engineering 200(47-48) (2011) 3410-3424

[46] H. Kapoor, R. Kapania, Geometrically nonlinear NURBS isogeometric finite element analysis of laminated composite plates, Composite Structures 94 (2012) 3434-3447

[47] T. Le-Manh, J. Lee, Postbuckling of laminated composite plates using NURBS-based isogeometric analysis, Composite Structures 109 (2014) 286-293

[48] Oliver Weeger, Utz Wever, Bernd Simeon, Isogeometric analysis of nonlinear Euler–Bernoulli beam vibrations, Nonlinear Dynamic 72 (2013) 813-835

[49] S. Hosseini, Joris JC. Remmers, Clemens V. Verhoosel, René de Borst, An isogeometric continuum shell element for non-linear analysis. Computer Methods in Applied Mechanics and Engineering 271 (2014) 1-22

[50] H.F. Tiersten, Linear piezoelectric plate vibrations, Plenum press, New York, 1969

[51] P. Phung-Van, T. Nguyen-Thoi, T. Le-Dinh, H. Nguyen-Xuan, Static and free vibration analyses and dynamic control of composite plates integrated with piezoelectric sensors and actuators by the cell-based smoothed discrete shear gap method (CS-FEM-DSG3), Smart Materials and Structures 22 (2013) 095026

[52] J.N. Reddy, Mechanics of laminated composite plates – Theory and Analysis, New York: CRC Press, 1997

[53] S.Y. Wang, S.T. Quek, K.K. Ang, Vibration control of smart piezoelectric composite plates, Smart Materials and Structures 10 (2001) 637-644

[54] S.Y. Wang, A finite element model for the static and dynamic analysis of a piezoelectric bimorph, International Journal of Solids and Structures 41 (2004) 4075-4096

[55] N.M. Newmark, A method of computation for structural dynamics, Journal of the Engineering

Mechanics Division ASCE 85 (1959) 67-94

[56] J.N. Reddy, Geometrically nonlinear transient analysis of laminated composite plates, AIAA Journal 21 (1983) 621-629

[57] K.J. Bathe, Finite element procedures, NJ: Prentice-Hall, 1996

[58] A. Pica, R.D. Wood, E. Hinton, Finite element analysis of geometrically nonlinear plate behaviour using a mindlin formulation, Computers and Structures 11 (1980) 203-215

[59] K.Y. Lam, X.Q. Peng, G.R. Liu, J.N. Reddy, A finite element model for piezoelectric composite laminates, Smart Materials and Structures 6 (1997) 583-591

[60] P. Heyliger, D.A. Saravanos, Exact free-vibration analysis of laminated plates with embedded piezoelectric layers, Journal of the Acoustical Society of America 98 (1995) 1547-1557

[61] T.J.R. Hughes, J.A. Evans, A. Reali, Finite Element and NURBS Approximations of Eigenvalue, Boundary-value, and Initial-value Problems, Computer Methods in Applied Mechanics and Engineering 272 (2014) 290–320

[62] J. Chen, D.J. Dawe, S. Wang, Nonlinear transient analysis of rectangular composite laminated plates, Composite Structures 49 (2000) 129-139

FIGURES

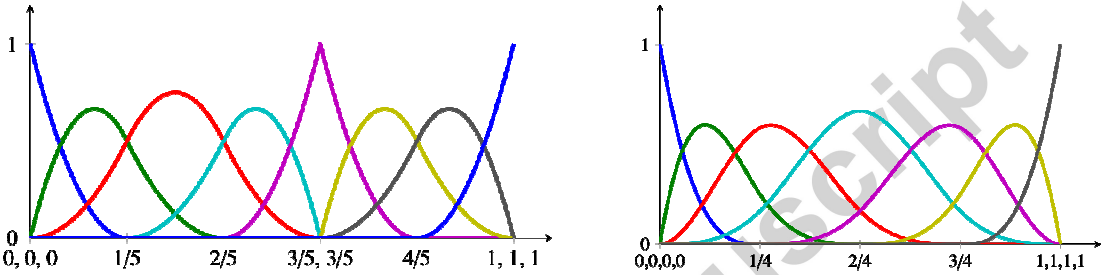

(a) (b)

Figure 1. B-splines basic functions: a) Univariate quadratic; b) Univariate cubic.

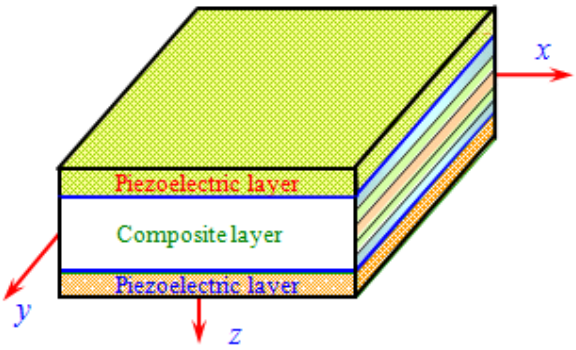

Figure 2. Configuration of a piezoelectric laminated composite plate.

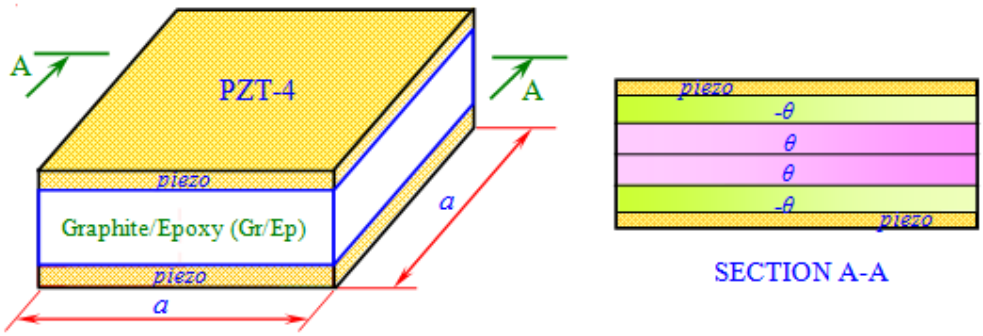

Figure 3. Square piezoelectric composite plate model.

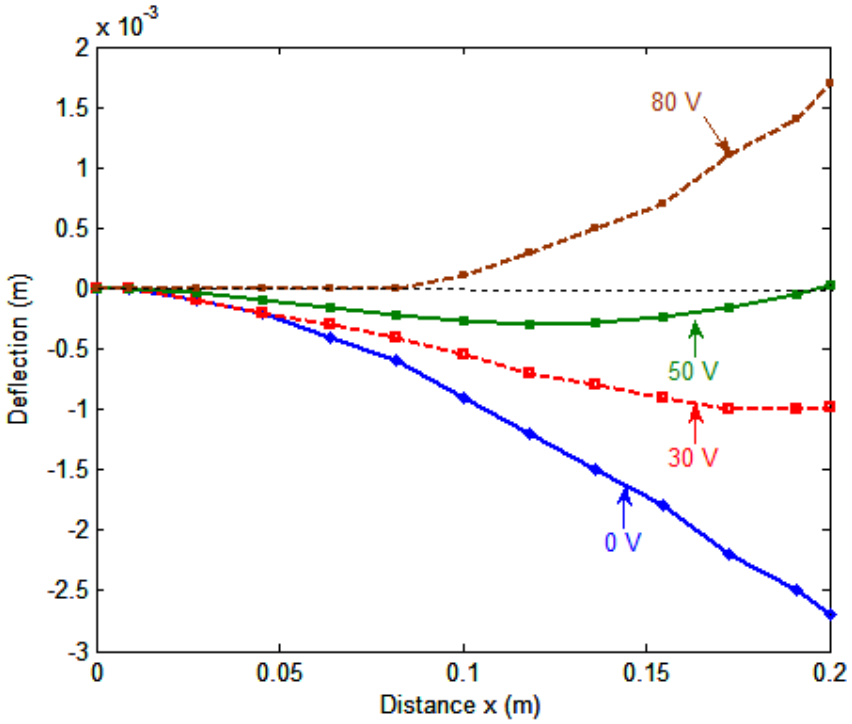

Figure 4. Effect of actuator input voltages on deflection of the piezoelectric composite plate $[pie/\text{-}45/45]_{as}$ subjected to a uniform loading.

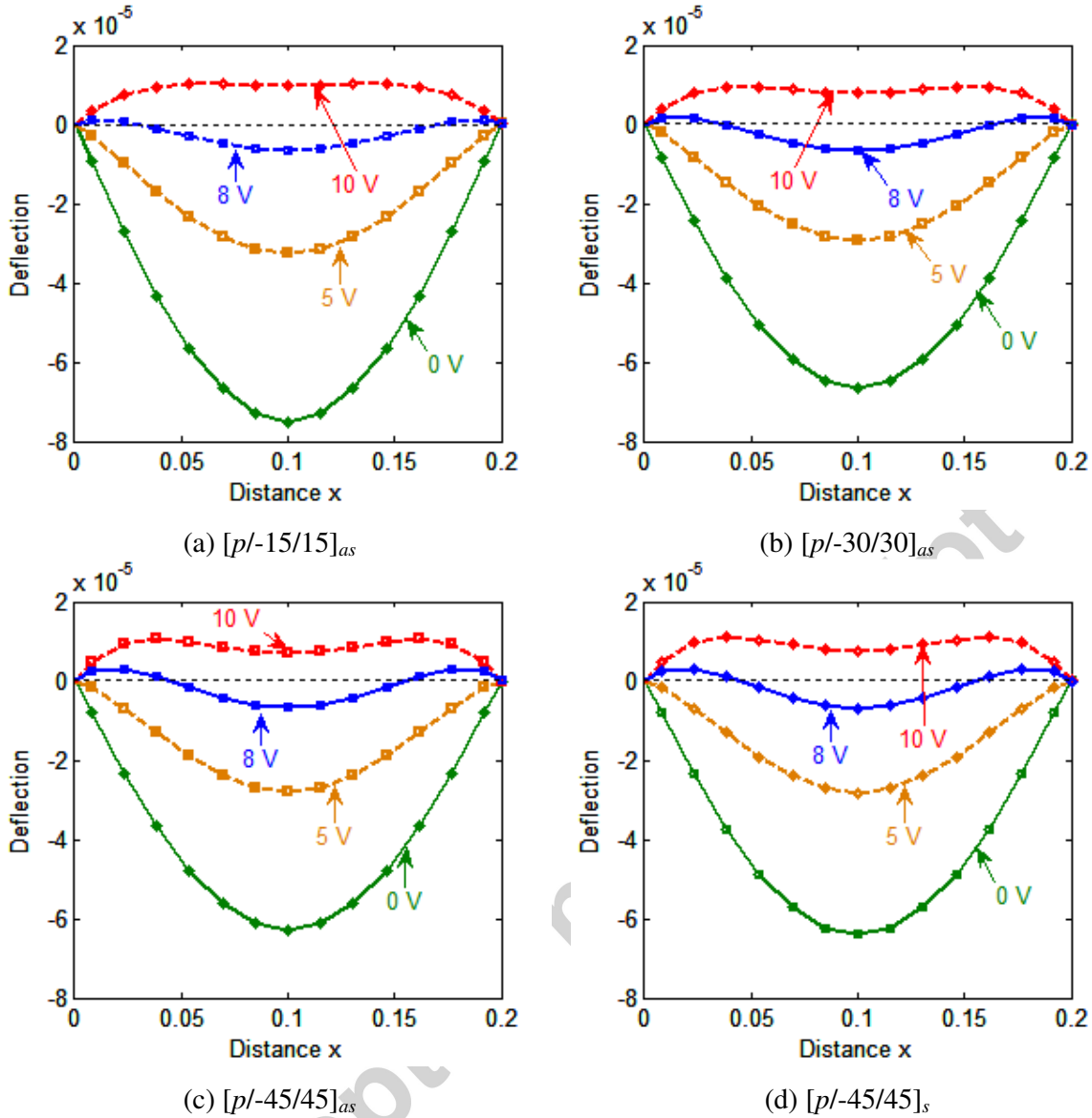

(a) $[p/\text{-}15/15]_{as}$ (b) $[p/\text{-}30/30]_{as}$

(c) $[p/\text{-}45/45]_{as}$ (d) $[p/\text{-}45/45]_{s}$

Figure 5. Centerline deflection of a simply supported piezoelectric composite plate subjected to uniform load and different input voltages.

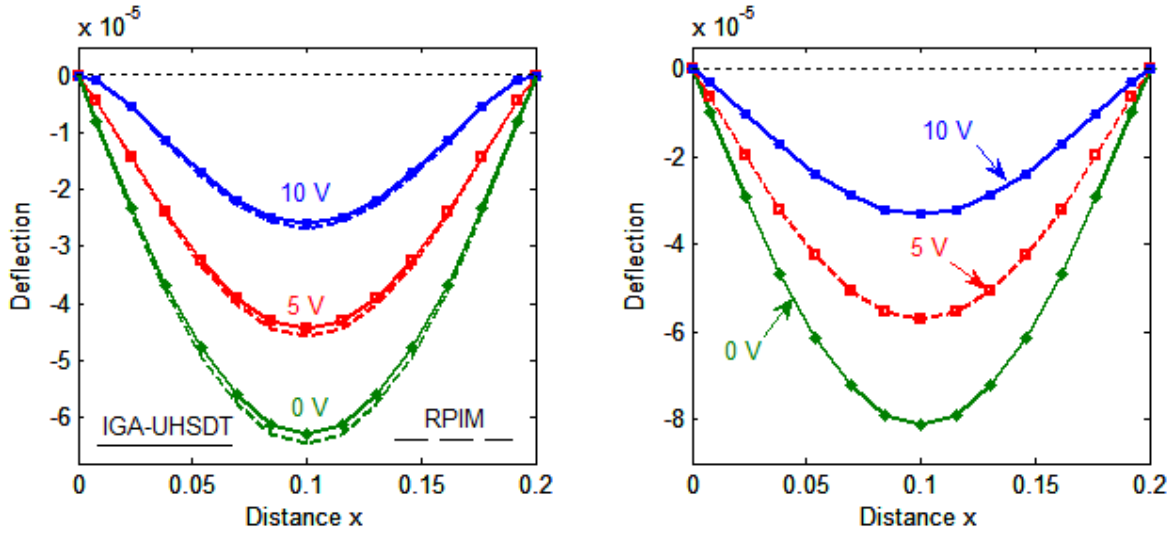

(a) $[-45/p/45]_{as}$ (b) $[-15/p/15]_{as}$

Figure 6. Effect of the stacking scheme and the fiber orientations on deflection of piezoelectric composite plate under uniform load and different input voltages.

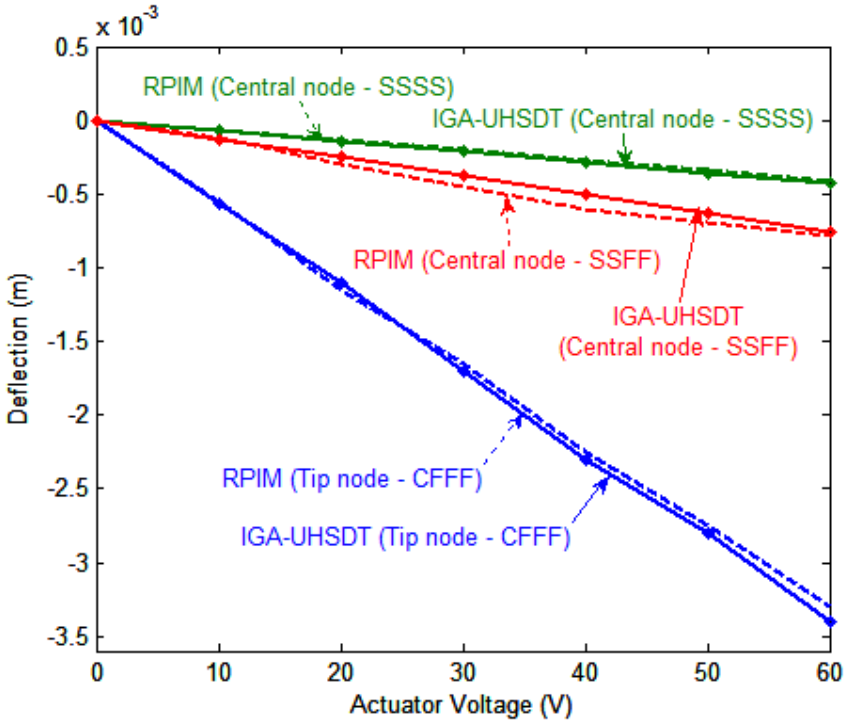

Figure 7. The deflection of the piezoelectric composite plates with various boundary conditions.

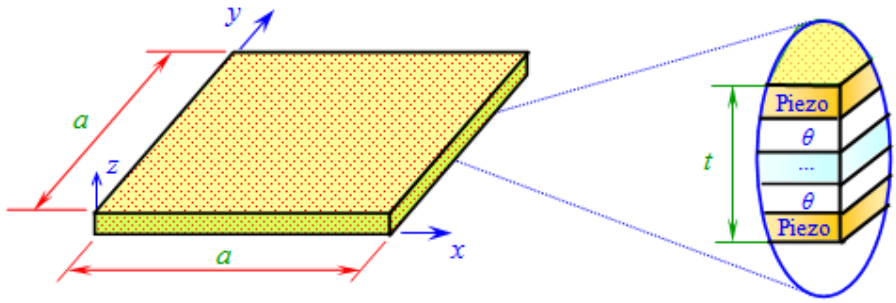

Figure 8. Model of an *n*-ply piezoelectric composite plate.

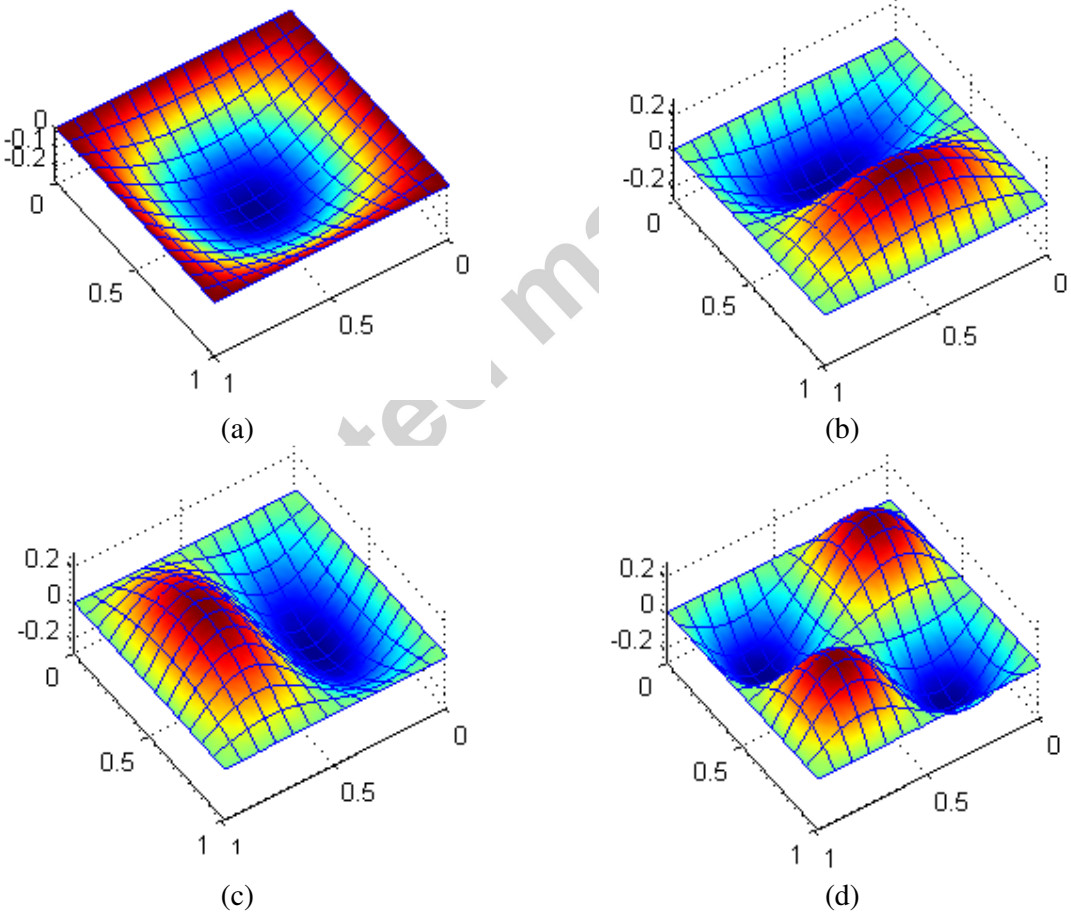

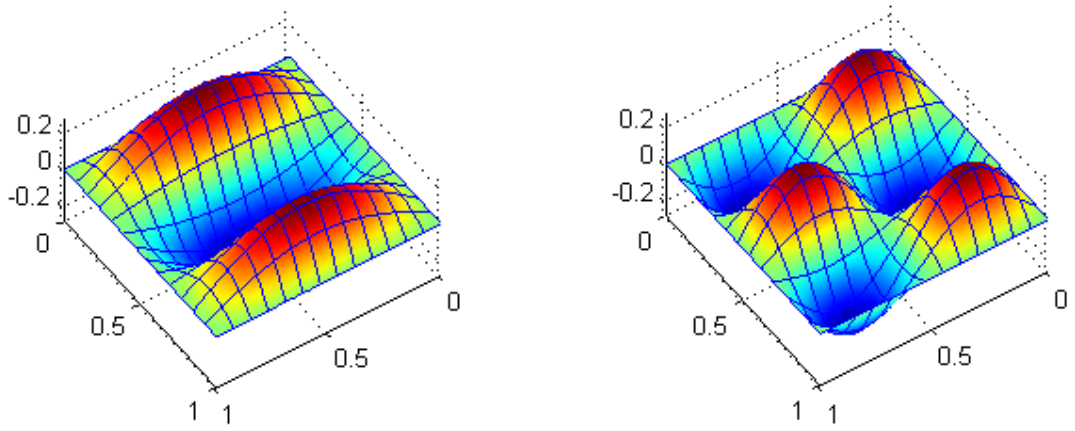

(e) (f)

Figure 9. Shape of the first six eigenmodes of a simply supported piezoelectric composite plate: (a) Mode 1; (b) Mode 2; (c) Mode 3; (d) Mode 4; (e) Mode 5; (f) Mode 6.

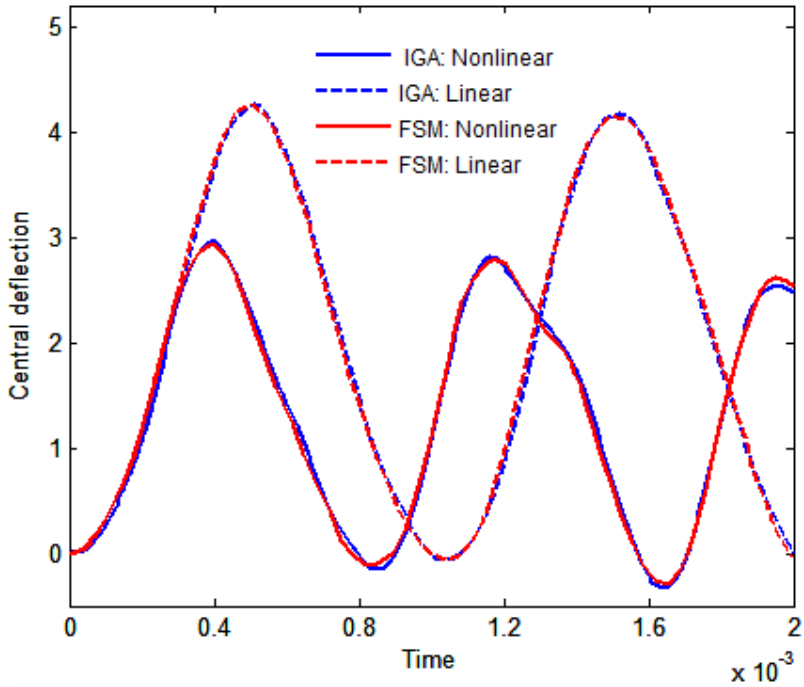

Figure 10. Normalized central defections of the plate under step uniform load

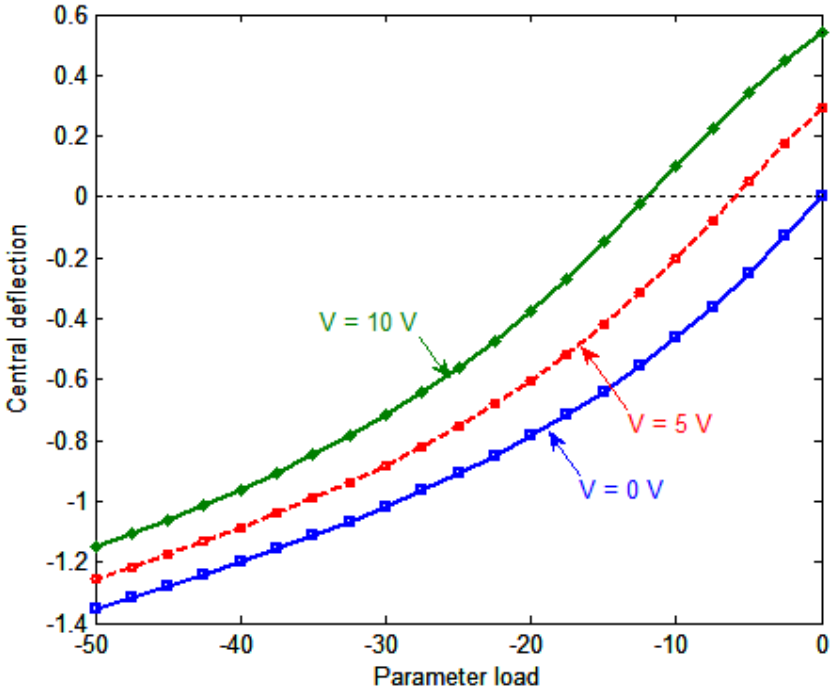

Figure 11. Effect of input voltages on nonlinear deflection of the piezoelectric composite plates [-45/*p*/45]*as*

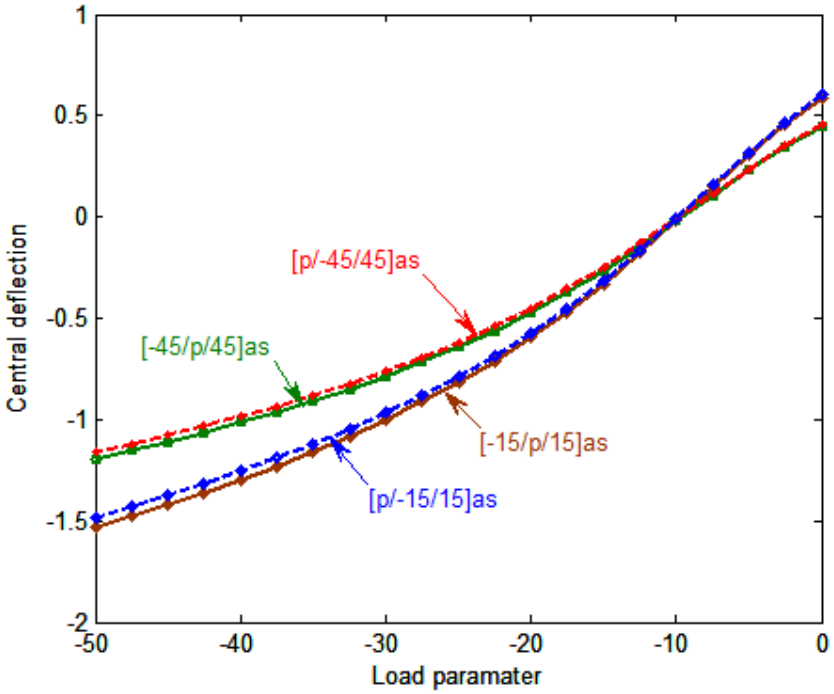

Figure 12. Effect of different fiber orientation angles on deflection of the plate subjected to input voltage 8V.

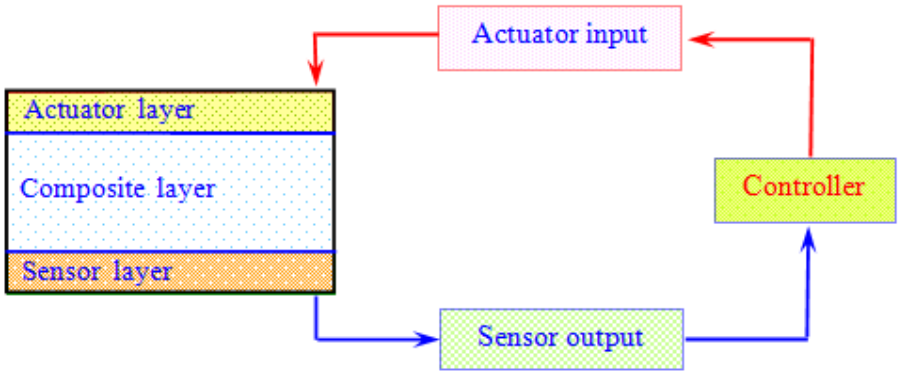

Figure 13. A schematic diagram of a laminated plate with integrated piezoelectric sensors and actuators.

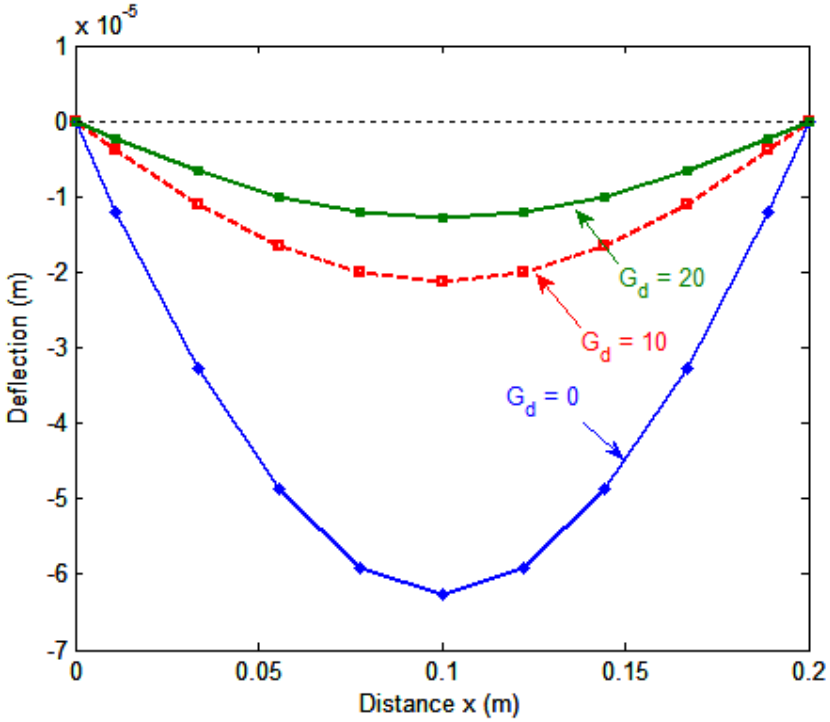

Figure 14. Effect of the gain G_d of the displacement feedback control on static deflections of the piezoelectric composite plate.

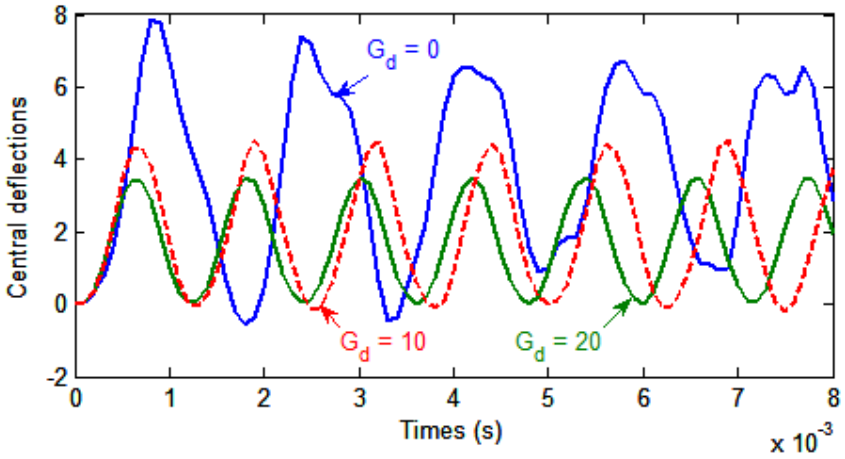

Figure 15. Effect of the control gain on the geometrically nonlinear response of the piezoelectric composite plate under step load.

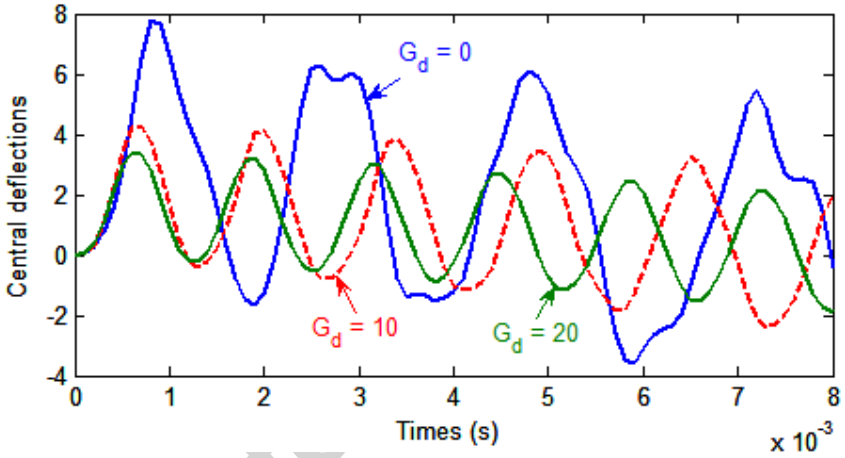

Figure 16. Effect of the control gain on the geometrically nonlinear response of the piezoelectric composite plate under triangular load.

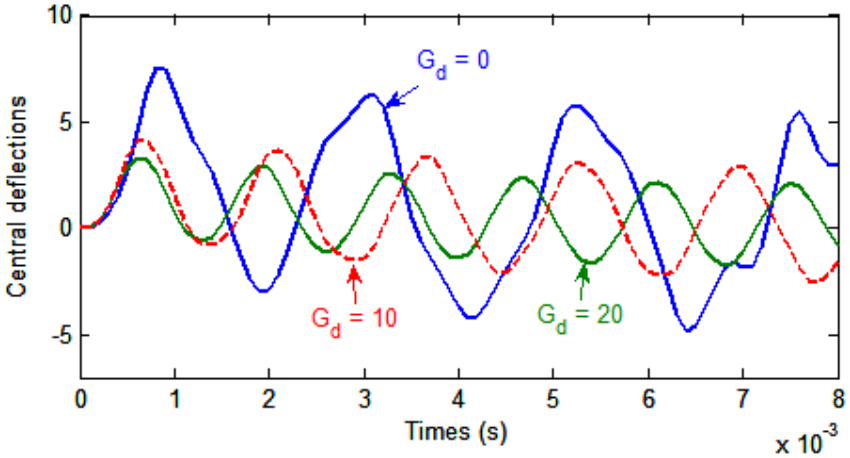

Figure 17. Effect of the control gain on the geometrically nonlinear response of the piezoelectric composite plate under explosive blast load.

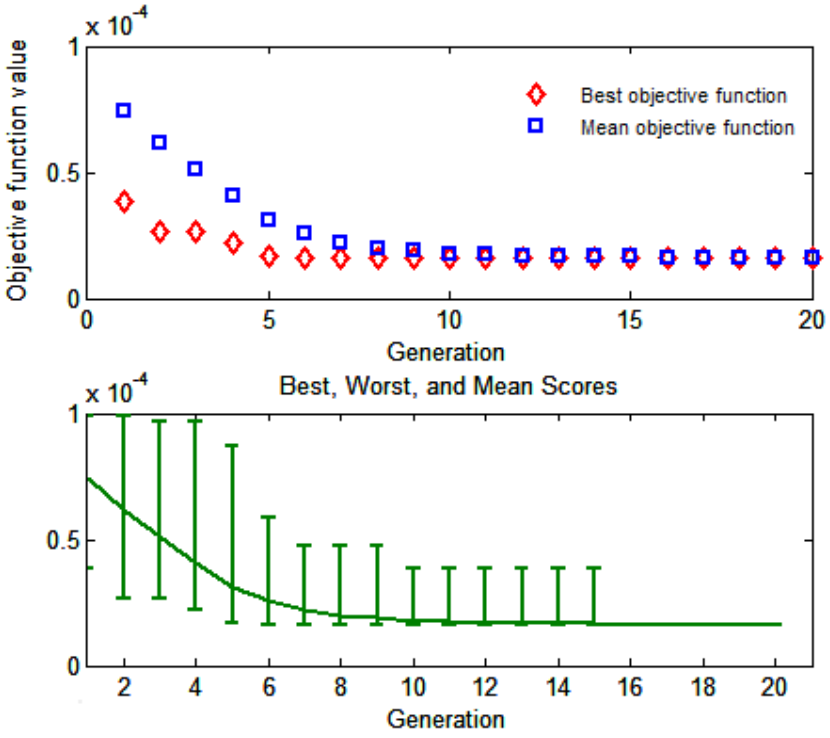

Figure 18. Convergence of objective function using GA with 20 generations.

TABLES

Table 1. Material properties of piezoelectric and composite materials.

Properties	PVDF	PZT-4	PZT-G1195N	T300/979	Gr/Ep
Elastic properties					
E_{11} (GPa)	2	81.3	63.0	150	132.38
E_{22} (GPa)	2	81.3	63.0	9.0	10.76
E_{33} (GPa)	2	64.5	63.0	9.0	10.76
G_{12} (GPa)	1	30.6	24.2	7.1	3.61
G_{13} (GPa)	1	25.6	24.2	7.1	5.65
G_{23} (GPa)	1	25.6	24.2	2.5	5.65
ν_{11}	0.29	0.33	0.30	0.3	0.24
ν_{23}	0.29	0.43	0.30	0.3	0.24
ν_{13}	0.29	0.43	0.30	0.3	0.49
Mass density					
ρ (kg/m^3)	1800	7600	7600	1600	1578
Piezoelectric coefficients					
$d_{31} = d_{32}$ (m/V)	0.046	-1.22e-10	2.54e-10	-	-
d_{15} (m/V)	-	-	-	-	-
Electric permittivities					
p_{11} (F/m)	0.1062e-9	1475	15.3e-9	-	-
p_{22} (F/m)	0.1062e-9	1475	15.3e-9	-	-
p_{33} (F/m)	0.1062e-9	1300	15.0e-9	-	-

Table 2. Central control point/node deflection of the simply supported piezoelectric composite plate subjected to a uniform load and different input voltages ($\times 10^{-4}$ m).

Input	Mesh	Method	Scheme			
			$[pie/\text{-}45/45]_s$	$[pie/\text{-}45/45]_{as}$	$[pie/\text{-}30/30]_{as}$	$[pie/\text{-}15/15]_{as}$
0V	5 x 5	IGA-UHSDT ($p = 2$)	-0.5618	-0.5634	-0.5940	-0.6611
		IGA-UHSDT ($p = 3$)	-0.6390	-0.6260	-0.6635	-0.7467
	9 x 9	IGA-UHSDT ($p = 2$)	-0.6174	-0.6082	-0.6441	-0.7236
		IGA-UHSDT ($p = 3$)	-0.6373	-0.6240	-0.6618	-0.7453
	13 x 13	IGA-UHSDT ($p = 2$)	-0.6322	-0.6202	-0.6576	-0.7401
		IGA-UHSDT ($p = 3$)	-0.6370	-0.6239	-0.6617	-0.7452
		RPIM [7]	-0.6038	-0.6217	-0.6542	-0.7222
5V	5 x 5	IGA-UHSDT ($p = 2$)	-0.1619	-0.1627	-0.1712	-0.1898
		IGA-UHSDT ($p = 3$)	-0.2856	-0.2827	-0.2975	-0.3279
	9 x 9	IGA-UHSDT ($p = 2$)	-0.2512	-0.2494	-0.2625	-0.2899
		IGA-UHSDT ($p = 3$)	-0.2847	-0.2819	-2.9701	-0.3287
	13 x 13	IGA-UHSDT ($p = 2$)	-0.2766	-0.2741	-0.2888	-0.3194
		IGA-UHSDT ($p = 3$)	-0.2842	-0.2817	-0.2968	-0.3283
		RPIM [7]	-0.2717	-0.2717	-0.2862	-0.3134
10V	5 x 5	IGA-UHSDT ($p = 2$)	0.2379	0.2380	0.2514	0.2815
		IGA-UHSDT ($p = 3$)	0.0678	0.0600	0.0685	0.0909
	9 x 9	IGA-UHSDT ($p = 2$)	0.1150	0.1093	0.1191	0.1437
		IGA-UHSDT ($p = 3$)	0.0680	0.0601	0.0677	0.0880
	13 x 13	IGA-UHSDT ($p = 2$)	0.0791	0.0721	0.0801	0.1013
		IGA-UHSDT ($p = 3$)	0.0690	0.0605	0.0682	0.0880
		RPIM [7]	0.0757	0.0604	0.0819	0.0954

Table 3. Dimensionless first natural frequency of the simply supported square piezoelectric composite plate [*pie*/0/90/0/*pie*].

Method	Meshing	Degrees of freedom (DOFs)	$\overline{f} = \omega_1 a^2 / \left(1000t\sqrt{\rho}\right)$	
			Closed circuit	Open circuit
IGA-UHSDT (*p*=2)	6 x 6	448	233.900	233.900
IGA-UHSDT (*p*=3)	6 x 6	567	231.400	231.400
IGA-UHSDT (*p*=4)	6 x 6	700	231.400	231.400
FEM layerwise [11]	12 x 12	2208	234.533	256.765
Q9 - HSDT [5]	-	-	230.461	250.597
Q9 - FSDT [5]	-	-	206.304	245.349
Reference solution [60]			245.941	245.942

Table 4. Convergence of five first natural frequencies of the square piezoelectric composite plate [*pie*/0/90/0/*pie*].

Mesh	Method	Mode sequence number				
		Mode 1	Mode 2	Mode 3	Mode 4	Mode 5
Open circuit						
5 × 5	IGA-UHSDT (p = 2)	236.00	594.50	741.3	1014.3	1531.8
	IGA-UHSDT (p = 3)	231.50	528.50	673.60	925.00	1128.7
	FE layerwise [11]	276.19	-	-	-	-
9 × 9	IGA-UHSDT (p = 2)	231.90	531.60	676.00	928.4	1087.8
	IGA-UHSDT (p = 3)	231.40	523.20	669.00	918.5	1030.0
	FE layerwise [11]	261.70	-	-	-	-
13 × 13	IGA-UHSDT (p = 2)	231.50	525.00	670.40	920.60	1040.1
	IGA-UHSDT (p = 3)	231.40	523.10	668.90	918.4	1027.9
	FE layerwise [11]	259.66	-	-	-	-
	Q9 - HSDT (11 dofs per node) [5]	250.50	583.19	695.70	980	1145.4
	Q9 - FSDT (5 dofs per node) [5]	245.35	559.00	694.20	962	1093.0
	Ref [60]	245.94	-	-	-	-
Closed circuit						
5 × 5	IGA-UHSDT (p = 2)	236.00	594.50	741.30	1014.3	1531.8
	IGA-UHSDT (p = 3)	231.50	528.50	673.60	925.00	1128.7
	FE layerwise [11]	249.86	-	-	-	-
9 × 9	IGA-UHSDT (p = 2)	231.90	531.60	676.00	928.40	1087.8
	IGA-UHSDT (p = 3)	231.40	523.20	669.00	918.50	1030.0
	FE layerwise [11]	236.83	-	-	-	-
13 × 13	IGA-UHSDT (p = 2)	231.50	525.00	670.40	920.00	1040.1
	IGA-UHSDT (p = 3)	231.40	523.10	668.90	918.40	1027.9
	FE layerwise [11]	234.53				
	Q9 - HSDT (11 dofs per node) [5]	230.46	520.38	662.92	908	1022.09
	Q9 - FSDT (5 dofs per node) [5]	206.30	519.44	663.34	908	1020.10
	Ref [60]	245.94	-	-	-	-

Table 5. The first ten natural frequencies of the square piezoelectric composite plate $[pie/-45/45]_{as}$

Mode	CFFF				SSSS			
	IGA-UHSDT		FEM [59]	RPIM [7]	IGA-UHSDT		FEM [59]	RPIM [7]
	$p = 2$	$p = 3$			$p = 2$	$p = 3$		
1	21.613	21.449	21.466	22.139	144.00	143.30	141.64	143.12
2	63.786	63.161	63.347	68.082	345.90	337.90	348.37	353.48
3	133.951	129.393	130.811	149.410	575.80	565.70	605.09	597.03
4	186.131	182.556	182.401	199.400	702.00	652.10	711.67	605.09
5	222.913	217.150	218.254	-	705.50	654.80	-	-
6	398.212	375.526	381.908	-	941.40	900.80	-	-
7	421.255	398.573	395.660	-	1273.70	1092.60	-	-
8	430.068	408.242	410.806	-	1322.90	1268.10	-	-
9	507.568	472.581	476.327	-	1507.10	1353.40	-	-
10	679.995	653.939	642.728	-	1887.60	1677.50	-	-

Table 6. Energy of plate with different input voltage and optimal input voltage.

Boundary condition	CFFF				
Actuator input voltages	0 V	30 V	50 V	80 V	20.7 (optimal)
Energy (J)	4.2476e-03	3.0362e-03	6.0570e-03	16.33e-03	2.67e-03
Boundary condition	SSSS				
Actuator input voltages	0 V	5 V	8 V	10 V	5.4 (optimal)
Energy (J)	10.37e-05	3.0670e-05	4.7090e-05	8.3139e-05	3.0249e-05

Highlights

- An efficient computational approach following a generalized unconstrained theory and isogeometric analysis (IGA) is proposed.
- It is then used for active control of nonlinear transient responses of smart piezoelectric composite plates.
- A procedure to search optimal design for actuator input voltages in piezoelectric plates is investigated.
- The numerical results demonstrate high efficiency of the present method.